Atmos. Meas. Tech. Discuss., 2, 2539–2586, 2009
www.atmos-meas-tech-discuss.net/2/2539/2009/

Atmospheric Measurement Techniques Discussions

Atmospheric Measurement Techniques Discussions is the access reviewed discussion forum of *Atmospheric Measurement Techniques*

Intercomparison of measurements of NO_2 concentrations in the atmosphere simulation chamber SAPHIR during the NO3Comp campaign

H. Fuchs[1,2,*], S. M. Ball[3], B. Bohn[4], T. Brauers[4], R. C. Cohen[5], H.-P. Dorn[4], W. P. Dubé[1,2], J. L. Fry[5], R. Häseler[4], U. Heitmann[6], R. L. Jones[7], J. Kleffmann[8], T. F. Mentel[4], P. Müsgen[4], F. Rohrer[4], A. W. Rollins[5], A. A. Ruth[6,9], A. Kiendler-Scharr[4], E. Schlosser[4], A. J. L. Shillings[7], R. Tillmann[4], R. M. Varma[6,9], D. S. Venables[9,10], G. Villena Tapia[8], A. Wahner[4], R. Wegener[4], P. J. Wooldridge[5], and S. S. Brown[1]

[1]National Oceanic and Atmospheric Administration, Earth System Research Laboratory, Boulder, CO, USA
[2]Cooperative Institute for Research in the Environmental Sciences, University of Colorado, Boulder, CO, USA
[3]Department of Chemistry, University of Leicester, Leicester, UK
[4]Institut für Chemie und Dynamik der Geosphäre 2, Forschungszentrum Jülich GmbH, Jülich, Germany

[5] Department of Chemistry, University of California Berkeley, Berkeley, CA, USA
[6] Department of Physics, University College Cork, Cork, Ireland
[7] Department of Chemistry, University of Cambridge, Cambridge, UK
[8] Physikalische Chemie/Fachbereich C, Bergische Universität Wuppertal, Wuppertal, Germany
[9] Department of Chemistry, University College Cork, Cork, Ireland
[10] Environmental Research Institute, University College Cork, Cork, Ireland
[*] now at: Institut für Chemie und Dynamik der Geosphäre 2, Forschungszentrum Jülich GmbH, Jülich, Germany

Received: 24 September 2009 – Accepted: 25 September 2009 – Published: 8 October 2009

Correspondence: S. S. Brown (steven.s.brown@noaa.gov)

Abstract

NO_2 concentrations were measured by various instruments during the NO3Comp campaign at the atmosphere simulation chamber SAPHIR at Forschungszentrum Jülich, Germany, in June 2007. Analytic methods included photolytic conversion with chemiluminescence (PC-CLD), broadband cavity ring-down spectroscopy (BBCRDS), pulsed cavity ring-down spectroscopy (CRDS), incoherent broadband cavity-enhanced absorption spectroscopy (IBBCEAS), and laser-induced fluorescence (LIF). All broadband absorption spectrometers were optimized for the detection of the main target species of the campaign, NO_3, but were also capable of detecting NO_2 simultaneously with reduced sensitivity. NO_2 mixing ratios in the chamber were within a range characteristic of polluted, urban conditions, with a maximum mixing ratio of approximately 75 ppbv. The overall agreement between measurements of all instruments was excellent. Linear fits of the combined data sets resulted in slopes that differ from unity only within the stated uncertainty of each instrument. Possible interferences from species such as water vapor and ozone were negligible under the experimental conditions.

1 Introduction

Nitrogen oxides, NO_x (=NO and NO_2), play a vital role in many aspects of the chemistry of the atmosphere. They influence ozone (O_3) and particulate matter formation and therefore air quality, contribute to acid deposition and form atmospheric oxidants such as the nitrate radical (NO_3). NO_x is emitted in combustion processes and also has natural sources such as lightning and soil. NO_x is mainly removed from the atmosphere via the formation of nitric acid (HNO_3) and its subsequent wet/dry deposition. In the absence of sunlight, the nitrate radical (NO_3) and its reservoir species, dinitrogen pentoxide (N_2O_5), become abundant nitrogen species. They are formed via the reactions of NO_2 with O_3 and with NO_3, respectively.

Because of its importance in atmosphere chemistry, many direct and indirect tech-

AMTD

2, 2539–2586, 2009

niques to measure NO_2 have been developed. Reduction of NO_2 to NO using a heated molybdenum catalyst or a photolytic converter followed by detecting the chemiluminescence of the reaction of NO with O_3 is the most common method (Kley and McFarland, 1980; Ryerson et al., 2000). Long path differential absorption (Platt et al., 1979; Platt and Stutz, 2008), diode laser based absorption (Lenth and Gehrtz, 1985; Sonnenfroh and Allen, 1996; Li et al., 2004) and fluorescence (Thornton et al., 2000; Matsumoto et al., 2001; Matsumi et al., 2001; Dari-Salisburgo et al., 2009) spectroscopy are approaches to detect NO_2 directly. During the last decade cavity ring-down spectroscopy (CRDS) and its related forms cavity enhanced absorption spectroscopy (CEAS) and cavity attenuated phase shift spectroscopy (CAPS) have become powerful techniques to detect atmospheric trace gases (Ball and Jones, 2003; Brown, 2003) and have also been applied to NO_2 detection. A pulsed laser system (Osthoff et al., 2006), continuous wave laser diodes (Mazurenka et al., 2003; Kasyutich et al., 2003; Wada and Orr-Ewing, 2005; Kasyutich et al., 2006; Courtillot et al., 2006), LEDs (Kebabian et al., 2005; Langridge et al., 2006; Gherman et al., 2008) and a xenon short-arc lamp (Venables et al., 2006) have been used as light sources.

Here, we report the intercomparison of five different NO_2 detection systems. This exercise was part of a larger intercomparison campaign of instruments for the detection of NO_3 and N_2O_5 (Dorn et al., 2009; Apodaca et al., 2009). Some of the participating instruments also had the capability to detect NO_2, whilst other NO_2-specific instruments (e.g. PC-CLD and LIF) were deployed to monitor NO_2 concentrations during the NO_3 experiments. Eleven experiments were carried out at the atmosphere simulation chamber SAPHIR at the Forschungszentrum Jülich, Germany, during summer 2007.

2 Instruments

2.1 Photolytic conversion/chemiluminescence detector (PC-CLD)

Detection of NO and NO_2 via chemiluminescence (CL) is a standard technique, which is widely used in field missions and air quality monitoring (Demerjian, 2000). Here, a modified commercial CL detector from Eco Physics took part in this campaign (CLD TR 780, Rohrer and Brüning, 1992). The CLD was placed inside a sea container underneath the chamber and sampled chamber air at a flow rate of 1 liter per minute through an approximately 6 m long (4 mm i.d., residence time 1 s) Teflon line.

NO was measured using a chemiluminescence detector (ECO Physics, model TR780) equipped with an improved fluorescence vessel similar to that described by Ridley et al. (1992), for detection of O_3 by chemiluminescence. NO_2 was converted to NO by an LED photolytic converter (Droplet Measurement Technologies, model BLC, photolysis volume 17 ml, wavelength 395±8 nm) with a conversion efficiency of about 50%. NO and NO_x were measured alternately by periodically switching off the LEDs. NO_2 mixing ratios were calculated by interpolating two subsequent NO_x measurements for the point of time when the NO mixing ratio was measured. This interpolation procedure reduced the effective time resolution by a factor of two compared to the repetition rate of measurements. The instrument was calibrated using NO standard gas mixtures (2 ppmv NO in N_2, BOC-Linde) and gas phase titration for NO_2. Calibrations were performed before and after the campaign. Calibration factors were similar and interpolated for the time of the campaign.

The effect of sensitivity changes by water vapor in the fluorescence vessel (linear in water vapor, e.g. 5% at 17 hPa partial pressure) and by oxidation of NO with ambient O_3 in the inlet line and inside the photolytic converter was corrected. This correction was linear in the ozone mixing ratio for most of the time (depending on the chemical conditions). The scale of this correction was e.g. 11% at 150 ppbv O_3.

Ozonolysis of olefins can cause fluorescence in addition to the NO chemiluminescence. Here, this interference is taken into account together with the measurement of

the dark signal of the PMT by regularly switching to a zero mode, during which the sampled air/ozone mixture passes a Teflon coated relaxation volume (Rohrer and Brüning, 1992).

The only known species that is efficiently photolyzed within the wavelength range emitted by the LEDs in the photolytic converter in addition to NO_2 is HONO. The yield of NO from HONO photolysis has been determined numerically from the spectrum of the LEDs. This interference is less than 5% compared to the photolysis of NO_2.

The accuracy of the chemiluminescence detector for NO_2 is determined by the accuracy of the NO standard (±5%) used for the calibration of the instrument and the NO_2 conversion efficiency (±5%) in the photolytic converter so that the overall uncertainty is ±7%. The accuracy of the NO_x calibration was additionally checked by comparing changes of NO and NO_2 concentrations to those of ozone (O_3 measured by a UV absorption instrument, ANSYCO O341M) during the photolysis of approximately 50 ppbv NO_2 in zero air inside the SAPHIR chamber as described in Bohn et al. (2005).

2.2 Laser-induced fluorescence (LIF)

The U.C. Berkeley LIF instrument is capable of simultaneous measurements of NO_2, total peroxy nitrates, total alkyl organic nitrates, and HNO_3. The basic implementation employed in this campaign follows from that of Thornton et al. (2000) and Day et al. (2002), but a much simpler, less expensive continuous-wave laser source centered at 408 nm (8 mW, Toptica Photonics DL100) was used instead of a Nd:YAG pumped dye laser system at 585 nm. The use of 408 nm light is advantageous because of its higher NO_2 absorption cross-section (≈10 times larger than at 585 nm). The laser was focused sequentially into two 40 pass White cells, allowing for two separate measurements of NO_2 concentrations (see below). In each cell, the resulting red shifted broadband NO_2 fluorescence was spectrally filtered with a long pass (> 650 nm) quartz dielectric filter, backed by a red glass filter to reduce the background from Rayleigh, Raman and laser scattering, and then imaged onto a red-sensitive photomultiplier tube (Hamamatsu H7421-50) mounted 90° to both the pump laser beam and the gas flow

directions.

In the present setup, additional spectroscopic interferences could not be monitored by tuning the laser on and off a spectral feature of NO_2. However, non-resonant LIF detection is still highly specific because the NO_2 absorption cross section is much larger than that of most other atmospheric trace gases at 408 nm and NO_2 is the only molecule likely to have strong red-shifted fluorescence. The only known significant interference for LIF detection of NO_2 is water vapor due to fluorescence quenching (Donnelly et al., 1979), decreasing the instrument's sensitivity as the water mixing ratio increases. An empirical correction factor of 3.5% per 1% change in absolute humidity which is based on laboratory measurements is applied to account for this humidity effect (Thornton et al., 2000).

The LIF instrument was housed in a temperature controlled container below the SAPHIR chamber. The instrument's inlet at the chamber consisted of 40 cm of 0.32 cm i.d. Teflon tube sampling at a rate of 3 slm. Immediately after the 40 cm tube, the pressure was reduced with a glass capillary orifice before the flow was split 4 ways to allow for heating the sampled air to 4 different temperatures in heated quartz tubes for the conversion of different nitrogen oxide classes to NO_2 (Day et al., 2002). The glass capillary and PFA connectors were heated to 40°C in an aluminum enclosure to minimize the accumulation of HNO_3 and alkyl nitrates on instrument tubing. Following the heaters, sampled gas flowed through approximately 20 m of 0.32 cm i.d. Teflon tube at 67 hPa to the LIF detection cells. Total residence time in the tube between the chamber and detection cell is estimated at 0.5 s.

The calibration factor for the instrument (counts s^{-1} $ppbv^{-1}$) was measured at the beginning and end of each day by overflowing the inlet with mixtures of zero air and NO_2 from a calibrated source. In a typical 5 min calibration routine, two mass flow controllers are used to produce mixtures of 0, 17.2, 34.3, and 68.7 ppbv NO_2 in dry zero air (from an NO_2 gas mixture of 10 ppmv in N_2), each of which are sampled into the instrument for approximately one minute. The NO_2 concentration in the cylinder was measured after the campaign by the PC-CLD and agreed with the concentration

stated by the manufacturer (10.0 ppmv±5%). The zero signal of the LIF system was determined every hour during experiments by overflowing the inlet with zero air.

The instrument's accuracy is directly linked to the accuracy of the calibration standard (±5%) and is further limited by the correction due to water quenching which adds an additional 2% uncertainty due to the combined uncertainties in water vapor quenching rates and the relative humidity measurement (Thornton et al., 2000). A detection limit (2σ) of approximately 80 pptv was calculated for 10 s of signal averaging. The additional uncertainty in the background signal is 10 pptv for 10 min averaging.

2.3 Cavity ring-down spectroscopy (CRDS)

The NOAA cavity ring-down instrument, which is capable of simultaneously measuring atmospheric NO_3, N_2O_5 and NO_2 (Dubé et al., 2006; Osthoff et al., 2006; Fuchs et al., 2008) was placed on a permanently installed, movable platform that allowed for positioning the instrument directly underneath the chamber floor. A short (40 cm) Teflon inlet line was inserted vertically from the top of the instrument into the chamber.

The CRDS instrument uses a pulsed Nd:YAG pumped dye laser system (repetition rate 50 Hz) to provide light at 662 nm which allows the detection of NO_3. In addition, a fraction (about 5%) of the 532 nm light from the Nd:YAG laser is used for the detection of NO_2. The 532 nm cavity mirrors are spaced 91 cm apart and have a reflectivity of 99.999%. The light which is transmitted through the end mirror of the cavities is detected by a photomultiplier tube. Following the laser pulse, the intensity decays exponentially owing to the mirror transmission, Rayleigh and Mie scattering of the light and due to trace gas absorption within the ring-down cavity. The concentration of the absorber (here: $[NO_2]$) can be calculated from the difference between the decay times with (τ) and without (τ_0) its presence in the cavity using its absorption cross section (σ_{NO_2}) at the probing wavelength (Brown, 2003):

$$[NO_2] = \frac{R_L}{c\sigma_{NO_2}} \left(\frac{1}{\tau} - \frac{1}{\tau_0} \right) \quad (1)$$

Here, c is the speed of the light and R_L is the ratio of the total cavity length to the length over which the absorber is present in the cavity. The latter is reduced because the volumes adjacent to the mirrors are purged with zero air in order to ensure their cleanliness. The value of R_L was determined in laboratory experiments (1.15±0.03) (Osthoff et al., 2006; Fuchs et al., 2008). The absorption cross section was remeasured after the campaign to be 1.51×10^{-19} cm^{-2}, a value that agrees with the spectrum of Voigt et al. (2002) convolved over the Nd:YAG laser linewidth. The updated value is approximately 4% larger than determined previously in Osthoff et al. (2006). No calibration, aside from this absorption cross section, was applied to the NO_2 concentrations during the campaign.

4 slm of air was sampled at reduced pressure of approximately 350 hPa. In order to determine the ring-down time constant (τ_0) in the absence of NO_2 and O_3 (Eq. 1), the inlet of the system was overflowed with zero air supplied by an additional line that was attached to the tip of the inlet for 5 to 10 s typically every 10 min.

The 532 nm cavity is placed downstream of a cavity in which NO_3 is detected at 662 nm. There are no significant wall losses for NO_2 in the instrument (Fuchs et al., 2008). Because the NO_3 absorption cross section at 532 nm is more than an order of magnitude larger than that of NO_2 (Yokelson et al., 1994), it is removed by using a 95 cm length of Nylon tubing which serves as a scrubber for NO_3 (Fuchs et al., 2008).

The only interference in this NO_2 detection is caused by optical extinction of ozone, whose absorption cross section is approximately 50 times smaller than that of NO_2 at this wavelength (Burkholder and Talukdar, 1994). The contribution of the ozone absorption to the extinction is calculated from a separate ozone concentration measurement (UV absorption photometer) and subtracted from the measured signal (Osthoff et al., 2006). Aerosol particles, which scatter light efficiently and would therefore constitute a large interference to a gas phase optical extinction measurement, are removed from the sampled air by a filter (Teflon, 25 µm thickness, 47 mm diameter, 2 µm pore size), which is placed in the inlet line. Previous laboratory measurements have shown

that there is no loss of NO_2 on the filter.

The accuracy of the NO_2 concentration is mainly limited by the uncertainty in the absorption cross section, ±3%, (Voigt et al., 2002) and the measurement of R_L, ±3%, (Fuchs et al., 2008). Contributions of measured pressure and temperature are negligible. In addition, the accuracy of the ozone concentration measurement which is used to correct for its extinction at 532 nm in this instrument has to be taken into account (Osthoff et al., 2006). At a maximum ozone mixing ratio of 230 ppbv during this campaign (10 June) the maximum contribution of the ozone measurement (accuracy ±5%) to the uncertainty of the NO_2 was 0.22 ppbv at NO_2 mixing ratios of 1 to 2 ppbv. However, the ratio between O_3 and NO_2 was lower for most of the experiments (3 to 20) and therefore, the contribution of the ozone subtraction to the uncertainty in the NO_2 concentration was typically less than 1%.

2.4 Broadband cavity ring-down spectroscopy (BBCRDS)

Broadband cavity ring-down spectroscopy (BBCRDS) uses light from a pulsed broadband laser to measure the absorption spectrum of samples contained within a high finesse optical cavity (Bitter et al., 2005; Ball and Jones, 2003). A multivariate fit of reference absorption cross sections to structured absorption features in the sample's absorption spectrum retrieves the concentration of the molecular absorber using an analysis similar to that developed for differential optical absorption spectroscopy (DOAS) (Platt, 1999). Although the BBCRDS instrument deployed at SAPHIR was optimized for detection of NO_3 via its 662 nm absorption band (Yokelson et al., 1994), absorption due to NO_2 and water vapor and aerosol extinction were also measured within the instrument bandwidth.

In the present BBCRDS instrument, light from a broadband dye laser (662 nm, FWHM: 16 nm, repetition rate: 20 Hz) pumped by a 532 nm Nd:YAG laser was directed into a 183 cm long ring-down cavity formed by two highly reflective mirrors (Los Gatos, peak reflectivity: 99.996% at 680 nm). To preserve the cleanliness of the mirrors' surfaces, the custom-built mirror mounts were purged by 0.5 slm of dry synthetic air, giving

a ratio of the cavity's total length to that over which the sample was present of $R_L = 1.05$. Sample gas was drawn from the SAPHIR chamber through four parallel Teflon tubes (i.d.: 3 mm, length: 40 cm) into the ring-down cavity, which consisted of a 19 mm internal diameter Teflon tube. The sample flow rate was 10.1 slm, corresponding to a residence time of 2.7 s in the instrument.

The light exiting the ring-down cavity was dispersed in wavelength and imaged onto a clocked CCD camera (XCam CCDRem2). The time evolution of individual ring-down events was recorded simultaneously at 512 different wavelengths, corresponding to 512 clocked rows on the CCD camera. Typically, fifty ring-down events were integrated on the CCD camera before the image was read to a computer for processing/storage. The sample's absorption spectrum was then calculated from sets of wavelength resolved ring-down times measured when the cavity contained the sample, $\tau(\lambda)$, and when back-flushed with dry zero air, $\tau_0(\lambda)$:

$$\alpha(\lambda) = \frac{R_L}{c}\left(\frac{1}{\tau(\lambda)} - \frac{1}{\tau_0(\lambda)}\right) = \sum_i \alpha_i(\lambda) + \alpha_{\text{con}}(\lambda) \quad (2)$$

where c is the speed of light, $\alpha_i(\lambda) = \sigma_i(\lambda)[i]$ is the absorption coefficient of the ith molecular absorber and $\alpha_{\text{con}}(\lambda)$ is the absorption coefficient due to all unstructured contributions to the spectrum (mainly aerosol extinction). Absorption spectra were averaged to a time resolution of 1 min and then fitted for the molecular absorption cross sections and a quadratic polynomial function to account for unstructured contributions. The NO_2 reference spectrum of Vandaele et al. (1996) was used, degraded to the 0.36 nm FWHM instrument resolution. The precision of concentrations was determined from the gradient error of a plot of the molecule's absorption coefficients against its absorption cross section. It was was typically 4 ppbv for NO_2 ($1\,\sigma$ uncertainty, 60 s averaging time). The reported concentrations have been corrected for exclusion of the sample from the purged volume of the cavity's mirror mounts and for dilution of the sample by a small leak of outside air into the cavity (≈6% of the total flow). Laboratory investigations showed that losses of NO_2 onto the instrument's internal surfaces were

negligible (Shillings, 2009).

The 648–675 nm wavelength range used for BBCRDS detection of NO_3 (the principal target of the SAPHIR measurements) is far from ideal for sensitive NO_2 detection because the differential absorption cross sections of NO_2 are rather small ($\Delta\sigma = 1\times10^{-20}$ cm^2 molecule^{-1}). Furthermore, the NO_2 and NO_3 differential cross sections are anti-correlated in this region (correlation coefficient: −0.7). Thus in order to preserve the quality of the NO_3 retrievals, fitting the BBCRDS spectra for an NO_2 contribution was only attempted when a strong NO_2 signal was expected, i.e. when NO_2 was present inside the SAPHIR chamber at concentrations above 10 ppbv. The sensitivity of the broadband instruments would have been better if they could have operated at shorter wavelengths. For example, excellent quantitative agreement was observed between the BBCRDS instrument and co-located (photolytic) chemiluminescence detection of NO_2 down to 0.5 ppbv when the BBCRDS instrument was operated in a 560–570 nm bandwidth during the Reactive Halogens in the Marine Boundary Layer (RHaMBLe) field campaign.

2.5 Incoherent broadband cavity enhanced spectroscopy (IBBCEAS)

The IBBCEAS setup was designed for use in the SAPHIR chamber and for subsequent field campaigns. Like cavity ring-down spectroscopy, IBBCEAS uses an optically stable cavity to measure the total extinction of a gaseous sample. Instead of observing the time dependence of the light intensity inside the cavity, the steady state intensity I of broadband light transmitted through the cavity is measured by means of a dispersive device (e.g. spectrometer/CCD) after the cavity. The total extinction, $\epsilon(\lambda)$, of the light is given by (Fiedler et al., 2003):

$$\epsilon(\lambda) = \frac{1-R}{L}\left(\frac{I_0(\lambda)}{I(\lambda)} - 1\right) \quad (3)$$

where I_0 is the intensity of the cavity without the sample, R is the effective mirror reflectivity, and L is the cavity length. The open path cavity was installed at the SAPHIR

chamber alongside the multi-pass DOAS instrument (see Fig. 1) such that the separation of the mirrors was much larger (20.13 m) than typically used in cavity ring-down or cavity-enhanced absorption spectroscopy (Varma et al., 2009). Since the mirrors were continuously purged with nitrogen at a flow rate of 10 l/h to retain their cleanliness, the effective cavity length was reduced to $L = (18.3 \pm 0.2)$ m. The measured extinction is described by a linear combination of relevant reference spectra and a broadband extinction represented by a second order polynomial that accounts for scattering and other unspecified loss processes. In this study the data from Burrows et al. (1998) were used as the reference absorption cross-section spectrum of NO_2. The wavelength range used for NO_2 retrievals was limited to the 630 to 645 nm region because the NO_2 absorption is the largest within the useable range of the spectrometer. In addition, the influence of water vapor is reduced in this region.

The details of the IBBCEAS setup at the SAPHIR chamber is described in Varma et al. (2009). The instrument consisted of a transmitter and a receiver unit placed at either end of the SAPHIR chamber. The transmitter unit housed a xenon short-arc lamp running in a so-called hot spot mode, which gave this lamp better imaging properties and spectral radiance compared to conventional xenon arc lamps. After wavelength selection (620 to 710 nm) by an interference filter and some beam shaping optical elements, the light was coupled into the cavity. The receiver unit contained the exit mirror of the cavity and included all optical elements in order to guide the transmitted light into the spectrometer (resolution 0.6 nm). An acquisition time of 5 s was used for all measurements.

In contrast with CRDS, the determination of trace gas concentrations (Eq. 3) by the IBBCEAS technique requires the knowledge of the mirror reflectivity. This is challenging for an open-path setup and for such a long cavity as used here. The mirror reflectivity was measured regularly by introducing an antireflection-coated optical substrate of known loss into the cavity. The absolute loss of the substrate was measured after the campaign by CRDS using a tunable dye laser system (Varma et al., 2009). The mirror reflectivity varied approximately 5×10^{-4} over the wavelength range between 620

to 680 nm. The value of the reflectivity was reproducible over the course of the campaign to within 3×10^{-4} at its maximum of approximately 0.9987 at 660 nm. The light intensity I_0 in a clean atmosphere was determined from measurements before trace gases were introduced into the chamber. This was typically in the morning, when the chamber had been purged overnight with high a flow rate of zero air to flush out all remaining impurities from the last experiment.

3 Experiments

The atmosphere simulation chamber SAPHIR at the Forschungszentrum Jülich, Germany, is a facility to investigate chemical processes using atmospheric concentration of reactants in a controlled environment. For instrument intercomparison exercises such as this work, chamber measurements are preferable to the ambient atmosphere, because the fast mixing of air in the chamber ensures that all instruments sample the same concentration of the test species and the measurements are less susceptible to unknown interferences that may be present in ambient air (e.g. Schlosser et al., 2007; Apel et al., 2008).

The chamber has been described in more detail elsewhere (e.g. Bohn et al., 2005; Rohrer et al., 2005; Wegener et al., 2007). It is of cylindrical shape (diameter 5 m, length 18 m, volume 270 m^3) and consists of a double wall FEP film. The chamber is operated at ambient temperature and pressure is slightly above that of the outside environment. Air, which is consumed by sampling of instruments and by wall leaks, is continuously replenished with zero air leading to a dilution of trace gases at approximately 5% per hour. The volume between the two Teflon walls is continuously purged with nitrogen to prevent ambient air diffusing through the chamber's Teflon walls. Between experiments, the chamber was flushed with zero air (quality 6.0) at high flow rates (up to 500 m^3/h) in order to remove trace gases to concentrations below the detection limit of instruments. Natural sunlight is used to establish photolytic reactions. A fast shutter system allows for operation of the chamber in darkness or ambient sun-

light. For the purpose of this campaign, the shutter system was only opened for short events (duration within the range of minutes), because NO_3, having been the main target species of the campaign, is easily photolyzed by visible light.

Trace gases such as NO_2 (from a gas mixture) or O_3 (produced by a silent discharge ozonizer) can be injected into the chamber. A fan that ensures rapid mixing (time scale of several minutes) was operated in almost all experiments. The chamber is equipped with a variety of instruments to monitor operational parameters and trace gas concentrations. A long path differential absorption spectrometer using a xenon arc lamp (DOAS) was also running using a spectral range between 603 and 691 nm. In principle, NO_2 concentrations could be retrieved from the broadband DOAS absorption measurements. However, the wavelength region was chosen for sensitive NO_3 detection, so that the limit of detection for NO_2 was higher than the NO_2 concentrations during the experiments for most of the time. Therefore DOAS data were not included in this intercomparison.

NO_2 instruments, which sampled air from the chamber through an inlet line, were placed underneath the chamber floor. The length of inlet lines varied between 40 cm (CRDS) and several meters (PC-CLD). The IBBCEAS setup was the only instrument that measured the optical extinction of inside the chamber using light paths parallel to the central long symmetry axis of the chamber. Figure 1 shows the arrangement of the NO_2 detectors included in this intercomparison.

Eleven experiments were conducted in the chamber. Chemical mechanisms for some of the experiments are discussed in separate papers (Fry et al., 2009; Rollins et al., 2009) and therefore are only briefly described here. An overview of NO_2 mixing ratios (shown at the native time resolution) and time series of some relevant key species, if added in the experiment, are shown in Figs. 2 and 3. A summary of chemical conditions is given in Table 1.

The majority of experiments were governed by the slow oxidation of NO_2 to NO_3 by O_3 in the dark chamber. Consequently, NO was not present under these conditions. NO_2 was introduced from a gas mixture in nitrogen (Linde) in all experiments. Inject-

ing NO_2 into the chamber took place at the beginning of experiments and lasted up to several minutes. Additional NO_2 was added at later times during some experiments. During one experiment (12 June) NO_2 was continuously added at a small flow rate over 3.5 h. Maximum NO_2 mixing ratios ranged from 3 to 75 ppbv during different experiments while minimum values subsequent to the initial addition were on the order of 0.2 ppbv (Figs. 2 and 3). O_3 was typically added to the gas mixture in the chamber at the same point in time as NO_2 in order to produce NO_3. O_3 mixing ratios were between 20 and 230 ppbv which was typically 3 to 20 times larger than the mixing ratio of NO_2.

Four experiments investigated the formation of NO_3 and N_2O_5 under various conditions which might influence the performance of the different instruments: a mixture of O_3 and NO_2 alone in dry air, (9 June), addition of water vapor (10 June), addition of inorganic aerosol (15 June) and short photolysis events (12/13 June). These experiments involved mainly the reactions during which NO_3 was formed and destroyed by photolysis:

$$NO_2 + O_3 \rightarrow NO_3 + O_2 \qquad \text{(R1)}$$

$$NO_3 + NO_2 \leftrightarrows N_2O_5 \qquad \text{(R2)}$$

$$NO_3 + h\nu \rightarrow NO_2 + O \quad (87\%) \qquad \text{(R3)}$$

$$NO_3 + h\nu \rightarrow NO + O_2 \quad (13\%) \qquad \text{(R4)}$$

The chemistry was complicated in five experiments by the addition of various volatile organic compounds: butanal (14 June), isoprene (18 June), limonene (16 June) and β-pinene under dry and humid conditions (20 and 21 June, respectively). These experiments were chosen to compare instruments under more complex conditions and to investigate the degradation of VOCs via the reaction with NO_3. Ambient air which was filtered of larger particles was filled into the chamber in one further experiment (11 June). NO_3 production was enhanced by adding NO_2 and O_3 after the chamber had been filled with ambient air.

4 Results and discussion

4.1 Time series of NO_2 mixing ratios

Figures 2 and 3 show time series of NO_2 mixing ratios as they were measured by all instruments with their original time resolutions. NO_2 mixing ratios of all instruments agree well. Differences in the scatter of measurements from single instruments reflect the precision of instruments, partly expected from the different time resolutions (CRDS: 1 s, IBBCEAS: 5 s, LIF: 10 s). Data were averaged to 1 min intervals for further analysis. The 1σ standard deviation was taken as a measure of the variance during that time window, unless the error propagation of the high resolution data was larger than the standard deviation. Data during the injection of trace gases and data from a period of three minutes after the injection, which is the mixing time in the chamber, were excluded from the analysis. Figure 4 shows all 1 min data which were included in the analysis.

Time series of NO_2 were similar in most of the experiments (Fig. 4). In nearly all experiments, the NO_2 concentration decreased over the course of the experiment, after the short initial injection of NO_2 into the chamber. In principle, the expected NO_2 concentration after the injection could be calculated from the added volume and the NO_2 concentration in the gas cylinder. However, flow controllers and the NO_2 concentration in the cylinder were not accurately calibrated for this campaign. As noted previously, NO_2 and other chamber constituents were continuously diluted at a rate of approximately 5% per hour (see e.g. 9 June between 10:00 and 10:30 LT). On 10 June water vapor was introduced into the chamber in several steps between 10:00 and 12:00 LT causing additional dilution steps, due to the amount of zero air required to facilitate filling the chamber with water vapor.

If O_3 was present, the oxidation of NO_2 to NO_3 and N_2O_5 led to an accelerated decrease of the NO_2 concentration (Reaction R1). For example, on 20 June at 09:00 LT the ozone mixing ratio was increased from 10 to nearly 100 ppbv (NO_2 was not added simultaneously at this time) resulting in a more rapid NO_2 decrease due to its increased

oxidation rate. During several experiments a rapid, small increase of the NO_2 mixing ratio was observed (16:00 LT 18 June, 09:30 LT 20 June, 10:45 LT 21 June). These were periods when hydrocarbons such as isoprene were introduced into the chamber. Since oxidation of hydrocarbons by NO_3 affects the equilibrium (Reaction R2), the rapid loss of NO_3 was followed by an increase in NO_2 mixing ratios due to the decomposition of N_2O_5 to NO_3 and NO_2 at constant temperature.

4.2 Comparison of instruments

Because PC-CLD instruments are widely used and have good sensitivity, PC-CLD measurements are taken as reference for this regression analysis. However, this does not imply that the PC-CLD results are correct; indeed, the results of the analysis are independent of the choice of reference. The NO_2 concentration was well above the detection limit during all experiments for CRDS, IBBCEAS, LIF, and PC-CLD, but was below the detection limit of BBCRDS during some of the experiments, which are excluded from the regression analysis. Tables 2 and 3 show results of the regression analysis for single experiments and for the combined data set. The fit procedure from Press et al. (1992) (FitExy procedure) accounts for errors in both coordinates. The errors of the regression parameters are generally very small and χ^2 of the fit results are large for nearly all experiments and instruments. This indicates that the deviation from a linear relationship is not explained by the error bars of the data. This can happen for two reasons: (1) error bars are underestimated and (2) there are non-linear deviations larger than the precision of data. This point is further discussed below.

PC-CLD and LIF measurements are highly correlated, R^2>99% (Fig. 5, Table 2). The regression of the combined data set results in a slope of 1.01 with an insignificant offset. The slope is expected to be close to unity, because the NO_2 concentration of the calibration standard, with which the LIF sensitivity was measured, was verified by the PC-CLD. The maximum deviations between these two instruments are observed on 14 June and 9 June, when LIF measurements are 6% lower and 7% higher than those by the PC-CLD, respectively. For some experiments (e.g. 18 June) time series of

LIF and PC-CLD show systematic differences in the slope of the continuously decreasing NO_2 concentration in the order of a few percent (less than the stated accuracy of instruments). This is observed over the whole course of one experiment or temporarily for minutes to hours (see e.g. 16 June). This may indicate small, temporary variations in the LIF or PC-CLD sensitivity.

NO_2 values reported by LIF are larger than those reported by PC-CLD and CRDS during the experiment on 12 June between 08:30 and 12:00 LT. A small flow of NO_2 constantly increased the NO_2 mixing ratio during this period in contrast to large, short additions in all of the other experiments. Although the fan was operated during the addition and therefore a mixing time of less than 1 min is expected, the observed difference in the NO_2 mixing ratio may have been due to an incomplete mixing of the air in the chamber resulting in a slightly higher local NO_2 concentration at the sampling point of the LIF instrument. Similar mixing effects are evident as differences in the short term (<5 min) response of the instruments to changes in NO_2 (Figs. 2 and 3).

The laser used for LIF has a fixed wavelength, so that this instrument has no real-time measure of potential interferences, whereas the previous dye laser version was tunable and thus interference signals could be measured by tuning the laser to a wavelength where NO_2 absorption is smaller. An in-situ comparison of NO_2 detection by the previous LIF system and PC-CLD has been reported in the literature including an extensive discussion of potential inlet interferences resulting from the conversion of NO_y to NO_2, as well as reaction of NO_2 with O_3 (Thornton et al., 2003). Water vapor, which is a quencher of NO_2 fluorescence in the LIF and the chemiluminescence in the PC-CLD instrument, was highly variable during the experiments (mixing ratios between 50 ppmv and 1.6%). Figure 6 shows the relative difference between LIF and CRDS measurements depending on the water vapor concentration in the chamber for all experiments during which water vapor was added. Because the reduction of the LIF signal is proportional to the LIF signal, the relative difference between LIF and CRDS measurements is plotted. CRDS measurements were taken as reference for this analysis, because there is no water vapor correction in contrast to measurements of the

PC-CLD. LIF measurements were corrected for water vapor quenching as described above and indeed there is no systematic dependence of the difference between measured NO_2 concentrations by LIF and CRDS observed in Fig. 6. This suggests that fluorescence quenching by water vapor is adequately taken into account in the evaluation of LIF measurements.

NO_2 concentrations measured by CRDS and PC-CLD also agree well (Fig. 5, Table 2) and exhibit high linear correlation (R^2>0.96 for all experiments). CRDS NO_2 values are scattered around those of PC-CLD (combined data set: −2%, maximum +3% on 9 June, minimum −4.5% on 12 and 21 June), but deviations are always smaller than the combined accuracies of both instruments (7% for PC-CLD, 6% for CRDS). There is also a small negative intercept of 0.1 ppbv for the entire data set. This most likely is caused by the uncertainty in the measurement of the zero ring-down time constant (Eq. 1).

As described above, CRDS measures the sum of NO_2 and O_3, thus ozone is an interference for the CRDS NO_2 detection. During experiments, when the ozone absorption was 20 to 50% of the extinction at 532 nm (9 June after 10:30 LT and 10 June after 14:00 LT), the difference between CRDS and PC-CLD NO_2 mixing ratios is larger than during experiments with smaller O_3 to NO_2 ratios. This demonstrates the lower accuracy and precision of CRDS measurements in the presence of high ozone due to the ozone subtraction in the calculation of the NO_2 absorption.

Figure 7 shows the difference between CRDS and PC-CLD NO_2 plotted against the ozone mixing ratio in order to test for artifacts in the subtraction of optical extinction from O_3 in the CRDS NO_2 measurement. Although this difference varies systematically with ozone during some individual experiments, there is no significant trend in the combined data set. Part of the trend observed during individual experiments may result from the covariance between NO_2 and O_3 themselves, since both species were typically introduced nearly simultaneously and were simultaneously consumed in the production of NO_3. Two observations support the accuracy of the ozone subtraction in the CRDS instrument. First, there is no change in the correlation between CRDS and PC-CLD

when the ozone mixing ratio was changed rapidly from 10 to nearly 100 ppbv on June 20 (Fig. 5). Second, there is no trend in the relative difference between CRDS and PC-CLD measurements in Fig. 7. This would be only the case either if there was no error in the ozone correction or if the error had the same dependence on the ozone concentrations as the NO_2 concentration (see Appendix).

Both the BBCRDS and IBBCEAS instruments use broadband light sources for the detection of NO_2. An accurate determination of NO_2 concentrations depends on the quality with which the absorption features of NO_2 can be measured and retrieved. These instruments were optimized for the detection of NO_3 around 660 nm, NO_3 being the primary target of this instrument intercomparison exercise. NO_2 absorbs in this wavelength region, too, albeit far less strongly than at shorter wavelengths. Thus a more sensitive NO_2 detection could be achieved if the broadband instruments had been optimized at wavelength of 400 to 500 nm where NO_2 has its largest differential absorption cross sections ($\Delta\sigma_{440\,nm} \approx 4\times10^{-19}$ cm^2 versus $\Delta\sigma_{660\,nm} \approx 0.1\times10^{-19}$ cm^2).

In the present study, NO_2 concentrations exceeded the limit of detection of BBCRDS only during three experiments, and concentrations were only well above their detection limits during the last two experiments (Table 3). Measurements are rather noisy, as shown in the correlation plot (Fig. 5). This agrees with the result that smaller correlation coefficients are found than for all other instruments. However, the fitted slope of the combined data set, 0.93, is close to unity and consistent with the accuracies of BBCRDS and PC-CLD (BBCRDS: 11%) showing the capability to retrieve reasonable NO_2 concentrations. Again, the precision of this instrument would be much improved in a different spectral region, so the current comparison represents a proof of concept more than a realistic evaluation of actual instrument performance when specifically targeting NO_2.

An IBBCEAS instrument with a cavity of similar length as the chamber was employed for the first time. Therefore, results of this campaign may not represent the performance of the instrument expected at a future stage of the development. The precision of IBBCEAS measurements is much higher compared to that of BBCRDS.

IBBCEAS instrument's spectral bandwidth extends further to short wavelengths providing access to stronger NO_2 absorption bands in the 630–645 nm window used for its NO_2 retrievals. Consequently the NO_2 concentrations were well above the detection limit of the IBBCEAS instrument for all experiments. Data from the second experiment (10 June) are excluded because instrumental parameters were optimized during this day and NO_2 retrievals are not reliable. The generally good agreement between IBBCEAS and PC-CLD measurements is more variable from experiment to experiment than observed for other instruments. Systematic drifts of IBBCEAS measurements within the range of several ppbvs are observed over the course of some experiments (Fig. 4). Nevertheless, IBBCEAS measurements are typically highly correlated with those of the PC-CLD as seen by the correlation coefficients, which are greater than 0.95 with two exceptions (Table 3). On 9 June, the NO_2 concentrations were the lowest in the campaign, approaching the precision of the IBBCEAS system (R^2=0.90), while on 15 June the correlation coefficient is significantly smaller, R^2=0.86, because IBBCEAS measurements are higher than those of the PC-CLD during the first hours, but are smaller during the second part of the experiment, after water has been added. Nevertheless, measurements of both instruments are well correlated before and after this event.

The variability in the slope of the regression most likely suggests that an instrumental parameter of the IBBCEAS instrument was not adequately determined at all times. Noise of the NO_2 values within the range of ±(3–5)% on a time scale of minutes to hours can be explained by the variability of the lamp intensity, which fluctuated within this range. The lamp intensity was indirectly monitored by observing the transmitted light in a wavelength region which is only influenced by broadband extinctions. However, the day-to-day variability of the slope in the regression is larger than these fluctuations and is likely related to the variability of another instrumental parameter. This hypothesis is supported by the fact that on days when NO_2 concentrations was determined by IBBCEAS are higher (up to 50%) than those of the other instruments (13, 20 and 21 June), deviations within this range (some 10%) are also observed for NO_3

mixing ratios between IBBCEAS and other instruments such as CRDS (Dorn et al., 2009).

Two parameters are required to calculate trace gas concentrations from the IBBCEAS measurement: (1) mirror reflectivity, R, and (2) light intensity, I_0, of the empty cavity (Eq. 3). R was only determined once a day. Since I_0 could only be determined in the clean cavity, this value was measured before trace gases were introduced into the chamber in the morning, when the chamber was filled with zero air. This was only possible before certain experiments (9, 12, 14, 16, and 21 June). I_0 values from the day after or before were used for evaluating measurements from the other experiments. Notably, positive differences between IBBCEAS and other instruments are the largest on days when I_0 was not measured on the same day. This indicates that the value I_0 is not valid for longer than 24 h as assumed in the evaluation.

4.3 Potential effects of the chamber on the intercomparison

It is interesting that at certain times IBBCEAS measurements differ from other measurements simultaneously with changes of the chamber status. IBBCEAS measured the average NO_2 concentration along the main symmetry axis of the chamber, while other instruments had inlet lines close to the Teflon floor. These periods occur when the fan inside the chamber was off (15:30–17:30 LT 9 June, 12:45–13:10 LT 12 June, 16:50–18:00 LT 12 June) with one exception (08:30–08:50 LT 15 June) and when the chamber roof was open for longer than 10 min (14:30–16:30 LT 11 June), whereas no significant change in the correlation between instruments are observed during short openings on 12/13 June, which are within the range of minutes.

The mixing time for trace gases in the dark chamber is much longer (on the order of 30 min) if the fan is not operated. The observed discontinuity between the average concentration from IBBCEAS and point measurements close to the chamber's floor from the other instruments may be the result of spatial inhomogeneity of trace gas concentrations. Several observations support this hypothesis. (1) During these periods, an increase in the NO_3 concentration of approximately 10% was observed by

all instruments. (2) A gradient of the NO_3 concentration was present within a layer of 40 cm to the chamber floor, which was not observed if the fan was operated. This was determined by test measurements in which the length of the inlet line of the CRDS instrument was varied.

4.4 NO_2 absorption cross section

For the retrieval of NO_2 concentrations from optical extinction measurements (BBCRDS, CRDS, IBBCEAS) different reference cross sections, σ_{NO_2} for NO_2 were used. For analysis of CRDS, the NO_2 cross section was determined independently as described above, but agrees to within 2% with the reference spectrum of Voigt et al. (2002). This agrees to within a few percent (within the wavelength region used here) with the reference data by Vandaele et al. (2002) applied for the evaluation of BBCRDS. Systematic differences between these instruments and PC-CLD and LIF, which are not based on an absorption measurement, are within the stated accuracy of the absorption cross sections, thus σ_{NO_2} in references Voigt et al. (2002) and Vandaele et al. (2002) are adequate for evaluating NO_2 absorption measurements. As pointed out by Orphal (2003), σ_{NO_2} from Burrows et al. (1998) used for IBBCEAS measurements is systematically 6–8% lower than reported by the more recent references above. The day-to-day variability of the correlation between IBBCEAS and the other instruments is larger than the difference in the absorption cross sections, such that this expected constant difference between data sets does not clearly emerge in the regression analysis. However, accounting for the difference in cross sections does bring the overall slope of the regression between IBBCEAS and PC-CLD measurements (Table 3) into significantly closer agreement within the PC-CLD and other techniques; for instance using the reference cross sections in Voigt et al. (2002) and Vandaele et al. (2002), respectively, would give an overall slope of approximately 1.10 instead of 1.19.

4.5 Precision of instruments

The limit of detection (LOD) of the instruments is calculated from statistics of measurements during periods when no NO_2 was present in the chamber by making an Allan deviation plot (Fig. 8). Two times the Allan deviation gives an estimate of the limit of detection of the instrument for a signal to noise ratio of two (S/N=2). The data set for BBCRDS does not include a sufficient number of zero measurements, in order to calculate a reasonable value for its limit of detection.

The PC-CLD exhibits the lowest limit of detection with 10 pptv (180 s, S/N=2), but for a longer integration time than all other instruments. In principle, a value within this range at a higher sampling rate can be achieved (Ryerson et al., 2000) at the costs of a higher experimental effort, but this is not required for measurements at the SAPHIR chamber, because concentrations are typically changing slowly during simulation experiments. The limit of detection of the other instruments at their native time resolution as determined from this campaign is 130 pptv for CRDS (1 s, S/N=2), 900 pptv for IBBCEAS (5 s, S/N=2), and 100 pptv for LIF (10 s, S/N=2). The Allan deviation for the CRDS instrument shows larger values than expected for pure random noise, so that the LOD (S/N=2) improves only to 80 pptv for 10 s averaged data. This is most likely due to the variability in the zero ring-down time constants (see above). In contrast, the Allan deviation for IBBCEAS and LIF behaves like random noise up to an averaging time of approximately 60 s, improving their LOD (S/N=2) to minimum values of 300 pptv and 50 pptv, respectively. The LOD can be compared for 10 s averaged data (except for PC-CLD). This is the minimum time resolution of the LIF instrument and data averaging behaves approximately like random noise for CRDS and IBBCEAS (Table 4). CRDS and LIF measurements show a similar LOD (S/N=2) of 80 and 100 pptv, respectively. IBBCEAS measurements exhibit the highest LOD (S/N=2) of approximately 600 pptv at this time resolution.

For the previous setup of the LIF instrument (Thornton et al., 2000) a limit of detection of 15 pptv at the same time resolution of 10 s and S/N=2 as used here has been

reported. Because the LIF instrument deployed in this campaign used a cw laser diode (see instrument description), the detector was not gated and its background signal was approximately 100 times higher than for the previous version of the system. In addition, the intensity of the cw diode laser was 10 times smaller than the average intensity of the pulsed laser system. The sum of these effects probably canceled out the advantages from the larger NO_2 absorption cross section at the shorter excitation wavelength of the new laser, so that the overall precision during this campaign is worse than reported in Thornton et al. (2000).

The 1σ precision observed for the CRDS instrument during this campaign is also smaller than previously reported by Osthoff et al. (2006) (80 pptv at 1 s) for a similar instrument. However, the laser used in this study was operated at a lower repetition rate, explaining approximately 65% of the observed increase. The remaining difference is possibly due to lower laser power.

In order to investigate the reason for the small errors of the parameters of the linear regression between data sets (see above), the precision of measurements at their native time resolution is also estimated for periods when either only NO_2, or NO_2 and O_3 was present in chamber. This value is expected to be similar to the error bars reported for the measurements. During these periods the NO_2 concentration decays as a single exponential function, so that the deviation of measurements from the expected ("real") NO_2 mixing ratio can be calculated by taking the residuum of a single exponential fit. To simplify the analysis, the standard deviation of the fit residuum for each of these periods is compared to the mean of the error bars of the reported data. The mean of the ratio between both values is shown in Table 4. The result indicates that the error bars (typically around 0.1 ppbv) reported for the CRDS data are underestimated by approximately 20%. They are determined from statistics of the measurement of the zero ring-down time constant (Eq. 1) and the fit error of the time constant, so that error bars in the CRDS data are a lower limit of their precision. However, errors in the fit parameters are still in the same order of magnitude, when the regression analysis is repeated with increased errors in the CRDS data, meaning that there is a small

non-linear relationship between CRDS and PC-CLD data.

In contrast, the precision as estimated from this analysis for measurements of the IBBCEAS and LIF instruments is better by approximately a factor of two than indicated by the reported error bars which range between 5 to 10% for LIF and 0.5 to 2 ppbv for IBBCEAS, respectively. This result is also supported by some of the calculated χ^2 values (Table 3), which are significantly smaller than the number of data points for some experiments (e.g. LIF 15 June, IBBCEAS 9 June). Thus, the small errors in the fit parameters cannot be explained by an underestimation of the precision of these instruments. Errors given for the IBBCEAS measurements are calculated from the different results obtained, if the spectra are fitted to different wavelength regions, and the fit error. Because it is not clear if the differences between concentrations derived for different wavelength regions are fully statistical or in part systematic, the error bars for IBBCEAS measurements are upper limits of the precision. Error bars for LIF measurements were calculated as standard deviations of 1 s data and hence it is expected that these errors show a realistic precision of data.

The comparison of error bars to the real precision of measurements show that the relationship between data sets over the course of an experiment and for the whole campaign cannot be explained by a unique linear relationship. This is most obviously demonstrated by the differing results of the regression analysis for different experiments. Changes in the linear relationship over the course of a single experiment are also larger than the instruments' native precision. This could be caused by e.g. small drifts in the instrument sensitivity. This behavior is rather small for CRDS and LIF measurements (compared to PC-CLD measurements), and is more distinct for data of the IBBCEAS instrument as already discussed above. However, this is a small deviation from a linear relationship in most cases as indicated by the high linear correlation coefficients and shows up only because of the high native precision of the measurements.

5 Conclusions

Five instruments capable of detecting NO_2 were compared in experiments at the atmosphere simulation chamber SAPHIR in Jülich, Germany. Experiments were designed to produce NO_3 at mixing ratios that are typical for nighttime conditions, so that NO_2 mixing ratios were also typical for atmospheric measurements. NO_2 concentration measurements between instruments that sampled through inlet lines close to the chamber's floor and instruments that measured the average along the symmetry axis of the chamber agreed well with the exception of periods when mixing in the chamber was reduced (i.e., mixing fan turned off) for test purposes. Otherwise, all instruments agreed to within their stated uncertainties. This study demonstrates again the usefulness of the SAPHIR chamber for intercomparison of instruments, since it is ensured that instruments sample air with the same concentration of the test species.

The two broadband detection systems performed NO_2 detection as a by-product of retrieving NO_3 concentrations in a wavelength range around 660 nm. As noted above, detection of NO_2 in this wavelength region is far from optimal because the NO_2 differential absorption cross sections are approximately 40 times smaller than peak values around 435 nm. Thus, the sensitivity of the broadband instruments would have been better if they had been operated at shorter wavelengths. Deviations in the slope of the regression are always smaller than the combined accuracies of instruments for the combined data set, but exceeded this limit for BBCRDS and IBBCEAS in some experiments, most likely showing day-to-day variability rather than any systematic errors. This will be improved in the future by more frequent monitoring of instrumental parameters of IBBCEAS and optimization of the BBCRDS sensitivity for a different wavelength region, if used for NO_2 detection.

The agreement between NO_2 mixing ratios from three other instruments, which are based on different techniques (chemiluminescence, fluorescence and absorption) and which are frequently used in field experiments, is better than 3%. This is smaller than the combined accuracies of these instruments. The high linear correlation coefficients

AMTD
2, 2539–2586, 2009

show that most of the variability in the scatter plot of combined data sets is explained by a linear relationship. This indicates that there were no significant interferences in the NO_2 detection of the different instruments for the conditions of this campaign. Known interferences, such as ozone for the 532 nm CRDS instrument and water vapor for LIF, were adequately taken into account in the data evaluation. Additional interferences would most likely lead to nonlinear correlations, unless concentrations of the interfering species and NO_2 were correlated or instruments suffered from the same interference. The precision of measurements for these instruments is high, resulting in small detection limits. However, small differences between measurements, which are larger than their precision, emerge over the course of the campaign, suggesting a small variability of the instrument sensitivities rather than an interference from other species.

In summary, this intercomparison demonstrated good performance of various NO_2 detection techniques used in field experiments. This increases the confidence in measurements of spectroscopy techniques for direct NO_2 detection which have not been widely used and validated such as chemiluminescence detectors. The technical expenses for these instruments are smaller than those required for PC-CLD measurements, in order to achieve highly accurate and precise NO_2 concentrations as demonstrated for experiments of this campaign. This shows their potential to compete with CLD instruments as routine measurements of NO_2 concentrations in the future.

Appendix A

Potential dependence of the relative difference between measurements on ozone

The NO_2 concentration, $[NO_2]^{ref}$, is a function of the ozone concentration (Fig. 7):

$$[NO_2]^{ref} = f(O_3)$$

It is assumed that the NO_2 concentration measured by one instrument (e.g. by CRDS), $[NO_2]$ scales with $[NO_2]^{ref}$ (slope, a, and negligible intercept) apart from an additional error that depends on the ozone concentration, $\epsilon(O_3)$:

$$[NO_2]=a[NO_2]^{ref} + \epsilon(O_3)$$

In this case, the dependence of the relative difference between both measurements can be expressed as:

$$\frac{[NO_2]-[NO_2]^{ref}}{[NO_2]^{ref}} = a\frac{[NO_2]^{ref}}{[NO_2]^{ref}} - \frac{f(O_3)}{[NO_2]^{ref}} + \frac{\epsilon(O_3)}{[NO_2]^{ref}} = a - 1 + \frac{\epsilon(O_3)}{f(O_3)}$$

This expression does not depend on the ozone concentration if $\epsilon(O_3)=0$ or if $\epsilon(O_3)=f(O_3)$. Since the latter case is unlikely it can be assumed that there is no systematic error that is related to ozone if no dependence of the relative difference on ozone is observed as it is the case for CRDS and CLD measurements shown in Fig. 7.

Acknowledgements. The NO_3-N_2O_5-Intercomparison campaign (2007) was supported by grant no. RII3-CT-2004-505968 of the European Community within the 6th Framework Program, Section Support for research Infrastructures – Integrated Infrastructure Initiative: EUROCHAMP and Priority 1.1.6.3. Global Change and Ecosystems: ACCENT. A. A. Ruth and D. S. Venables gratefully acknowledges support by the SFI STTF programme (contract no. 06/RFP/CHP055 STTF 08). Authors associated with University College Cork would like to thank the Irish EPA (contract no. 2005-ET-MS-28-M3) for supporting this project. Authors associated with University of California Berkeley would like to acknowledge support by NSF grants ATM-0639847 and ATM-0511829.

References

Apel, E. C., Brauers, T., Koppmann, R., Bandowe, B., Bossmeyer, J., Holzke, C., Tillmann, R., Wahner, A., Wegener, R., Brunner, A., Jocher, M., Ruuskanen, T., Spirig, C., Steigner, D., Steinbrecher, R., Gomez Alvarez, E., Müller, K., Burrows, J. P., Schade, G., Solomon, S. J.,

Ladstätter-Weissenmayer, A., Simmonds, P., Young, D., Hopkins, J. R., Lewis, A. C., Legreid, G., Reimann, S., Hansel, A., Wisthaler, A., Blake, R. S., Ellis, A. M., Monks, P. S., and Wyche, K. P.: Intercomparison of oxygenated volatile organic compound measurements at the SAPHIR atmosphere simulation chamber, J. Geophys. Res., 113, D20307, doi:10.1029/2008JD009865, 2008. 2552

Apodaca, R. L., Dorn, H.-P., Brauers, T., Brown, S. S., Cohen, R. C., Crowley, J. N., Dubé, W. P., Fry, J. L., Fuchs, H., Häseler, R., Kato, S., Kajii, Y., Kleffmann, J., Kiendler-Scharr, A., Labazan, I., Matsumoto, J., Nishida, S., Rohrer, F., Rollins, A. W., Schlosser, E., Schuster, G., Tillmann, R., Villena, G., Wahner, A., Wegener, R., Wooldridge, P. J., and Simpson, W. R.: Intercomparison of N_2O_5 sensors using the SAPHIR reaction chamber, Atmos. Chem. Phys. Discuss., in preparation, 2009. 2542

Ball, S. M. and Jones, R. L.: Broad-band cavity ring-down spectroscopy, Chem. Rev., 103, 5239–5262, doi:10.1021/cr020523k, 2003. 2542, 2548

Bitter, M., Ball, S. M., Povey, I. M., and Jones, R. L.: A broadband cavity ringdown spectrometer for in-situ measurements of atmospheric trace gases, Atmos. Chem. Phys., 5, 2547–2560, 2005, http://www.atmos-chem-phys.net/5/2547/2005/. 2548

Bohn, B., Rohrer, F., Brauers, T., and Wahner, A.: Actinometric measurements of NO_2 photolysis frequencies in the atmosphere simulation chamber SAPHIR, Atmos. Chem. Phys., 5, 493–503, 2005, http://www.atmos-chem-phys.net/5/493/2005/. 2544, 2552

Brown, S. S.: Absorption spectroscopy in high-finesse cavities for atmospheric studies, Chem. Rev., 103, 5219–5238, doi:10.1021/cr020645c, 2003. 2542, 2546

Burkholder, J. B. and Talukdar, R. K.: Temperature dependence of the ozone absorption spectrum over the wavelength range 410 to 760 nm, Geophys. Res. Lett., 21, 581–584, 1994. 2547

Burrows, J. P., Dehn, A., Deters, B., Himmelmann, S., Richter, A., Voigt, S., and Orphal, J.: Atmospheric remote-sensing reference data from GOME: Part 1. Temperature-dependent absorption cross-sections of NO_2 in the 231–794 nm range, J. Quant. Spectrosc. Ra., 60, 1025–1031, 1998. 2551, 2562

Courtillot, I., Morville, J., Motto-Ros, V., and Romanini, D.: Sub-ppb NO_2 detection by optical feedback cavity-enhanced absorption spectroscopy with a blue diode laser, Appl. Phys. B, 85, 407–412, doi:10.1007/s00340-006-2354-3, 2006. 2542

Dari-Salisburgo, C., Di Carlo, P., Giammaria, F., Kajii, Y., and D'Altorio, A.: Laser induced fluorescence instrument for NO_2 measurements: Observations at a central Italy background site, Atmos. Environ., 43, 970–977, doi:10.1016/j.atmosenv.2008.10.037, 2009. 2542

Day, D. A., Wooldridge, P. J., Dillon, M. B., Thornton, J. A., and Cohen, R. C.: A thermal dissociation laser-induced fluorescence instrument for in situ detection of NO_2, peroxy nitrates, alkyl nitrates, and HNO_3, J. Geophys. Res., 107, 4046, doi:10.1029/2001JD000779, 2002. 2544, 2545

Demerjian, K. L.: A review of national monitoring networks in North America, Atmos. Environ., 34, 1861–1884, 2000. 2543

Donnelly, V. M., Keil, D. G., and Kaufman, F.: Fluorescence lifetime studies of NO_2. III. Mechanism of fluorescence quenching, J. Chem. Phys., 71, 659–673, 1979. 2545

Dorn, H.-P., Apodaca, R. L., Ball, S. M., Brauers, T., Brown, S. S., Cohen, R. C., Crowley, J. N., Dubé, W. P., Fry, J. L., Fuchs, H., Häseler, R., Heitmann, U., Jones, R. L., Kato, S., Kajii, Y., Kiendler-Scharr, A., Labazan, I., Langridge, J. M., Matsumoto, J., Meinen, J., Nishida, S., Platt, U., Pöhler, D., Rohrer, F., Rollins, A. W., Ruth, A. A., Schlosser, E., Schuster, G., Shillings, A. J. L., Simpson, W. R., Thieser, J., Venables, D. S., Wahner, A., Wegener, R., and Wooldridge, P. J.: Intercomparison of NO_3 radical detection instruments in the Atmosphere Simulation Chamber SAPHIR, Atmos. Chem. Phys. Discuss., in preparation, 2009. 2542, 2561

Dubé, W. P., Brown, S. S., Osthoff, H. D., Nunley, M. R., Cicora, S. J., Paris, M. W., McLaughlin, R. J., and Ravishankara, A. R.: Aircraft instrument for simultaneous, in situ measurement of NO_3 and N_2O_5 via pulsed cavity ring-down spectroscopy, Rev. Sci. Instrum., 77, 034101, doi:10.1063/1.2176058, 2006. 2546

Fiedler, S. E., Hese, A., and Ruth, A. A.: Incoherent broad-band cavity-enhanced absorption spectroscopy, Chem. Phys. Lett., 371, 284–294, doi:10.1016/S0009-2614(03)00263-X, 2003. 2550

Fry, J. L., Kiendler-Scharr, A., Rollins, A. W., Wooldridge, P. J., Brown, S. S., Fuchs, H., Dub, W., Mensah, A., dal Maso, M., Tillmann, R., Dorn, H.-P., Brauers, T., and Cohen, R. C.: Organic nitrate and secondary organic aerosol yield from NO_3 oxidation of β-pinene evaluated using a gas-phase kinetics/aerosol partitioning model, Atmos. Chem. Phys., 9, 1431–1449, 2009, http://www.atmos-chem-phys.net/9/1431/2009/. 2553

Fuchs, H., Dubé, W. P., Ciciora, S. J., and Brown, S. S.: Determination of inlet transmission and conversion efficiencies for in situ measurements of the nocturnal nitrogen oxides, NO_3,

N_2O_5 and NO_2, via pulsed cavity ring-down spectroscopy, Anal. Chem., 80, 6010–6017, doi:10.1021/ac8007253, 2008. 2546, 2547, 2548

Gherman, T., Venables, D. S., Vaughan, S., Orphal, J., and Ruth, A. A.: Incoherent broadband cavity-enhanced absorption spectroscopy in the near-ultraviolet: Application to HONO and NO_2, Environ. Sci. Technol., 42, 890–895, doi:10.1021/es0716913, 2008. 2542

Kasyutich, V. L., Bale, C. S. E., Canosa-Mas, C. E., Pfrang, C., Vaughan, S., and Wayne, R. P.: Cavity-enhanced absorption: detection of nitrogen dioxide and iodine monoxide using a violet laser diode, Appl. Phys. B, 76, 691–697, doi:10.1007/s00340-003-1153-3, 2003. 2542

Kasyutich, V. L., Martin, P. A., and Holdsworth, R. J.: Phase-shift off-axis cavity-enhanced absorption detector for nitrogen oxide, Meas. Sci. Technol., 17, 923–931, doi:10.1088/0957-0233/17/4/044, 2006. 2542

Kebabian, P. L., Herndon, S. C., and Freedman, A.: Detection of nitrogen dioxide by cavity attenuated phase shift spectroscopy, Anal. Chem., 77, 724–728, doi:10.1021/ac048715y, 2005. 2542

Kleffmann, J., Gavriloaiei, T., Elshorbany, Y., Ródenas, M., and Wiesen, P.: Detection of nitric acid (HNO_3) in the atmosphere using the LOPAP technique, J. Atmos. Chem., 58, 131–149, doi:10.1007/s10874-007-9083-9, 2007.

Kley, D. and McFarland, M.: Chemiluminescence detector for NO and NO_2, Atmos. Tech., 12, 63–69, 1980. 2542

Langridge, J. M., Ball, S. M., and Jones, R. L.: A compact broadband cavity enhanced absorption spectrometer for detection of atmospheric NO_2 using light emitting diodes, Analyst, 131, 916–922, doi:10.1039/b605636a, 2006. 2542

Lenth, W. and Gehrtz, M.: Sensitive detection of NO_2 using high-frequency heterodyne spectroscopy with a GaAlAs diode laser, Appl. Phys. Lett., 47, 1263–1265, 1985. 2542

Li, Y. Q., Demerjian, K. L., Zahniser, M. S., Nelson, D. D., McManus, J. B., and Herndon, S. C.: Measurement of formaldehyde, nitrogen dioxide, and sulfur dioxide at Whiteface Mountain using a dual tunable diode laser system, J. Geophys. Res., 109, D16S08, doi:10.1029/2003JD004091, 2004. 2542

Matsumi, Y., Murakami, S., Kono, M., Takahashi, K., Koike, M., and Kondo, Y.: High-sensitivity instrument for measuring atmospheric NO_2, Anal. Chem., 73, 5485–5493, doi:10.1021/ac010552f, 2001. 2542

Matsumoto, J., Hirokawa, J., Akimoto, H., and Kajii, Y.: Direct measurement of NO_2 in the marine atmosphere by laser-induced fluorescence technique, Atmos. Environ., 35, 2803–

2814, 2001. 2542
Mazurenka, M. I., Fawcett, B. L., Elks, J. M. F., Shallcross, D. E., and Orr-Ewing, A. J.: 410-nm diode laser cavity ring-down spectroscopy for trace detection of NO_2, Chem. Phys. Lett., 367, 1–9, 2003. 2542
Orphal, J.: A critical review of the absorption cross-sections of O_3 and NO_2 in the ultraviolet and visible, J. Photochem. Photobiol., 157, 185–209, doi:10.1016/S1010-6030(03)00061-3, 2003. 2562
Osthoff, H., Brown, S. S., Ryerson, T. B., Fortin, T. J., Lerner, B. M., Williams, E. J., Petterssson, A., Baynard, T., Dubé, W. P., Ciciora, S. J., and Ravishankara, A. R.: Measurement of atmospheric NO_2 by pulsed cavity ring-down spectroscopy, J. Geophys. Res., 111, D12305, doi:10.1029/2005JD006942, 2006. 2542, 2546, 2547, 2548, 2564
Platt, U.: Modern methods for the measurement of atmospheric trace gases, Phys. Chem. Chem. Phys., 1, 5409–5415, 1999. 2548
Platt, U. and Stutz, J.: Differential Optical Absorption Spectroscopy, Principles and Applications, Springer, Berlin, 2008. 2542
Platt, U., Perner, D., Winer, A. M., and Pätz, H. W.: Simultaneous measurement of atmospheric CH_2O, O_3, and NO_2 by differential optical-absorption, J. Geophys. Res., 84, 6329–6335, 1979. 2542
Press, W. H., Teukolsky, S. A., Vetterling, W. T., and Flannery, B. P.: Numerical Recipies in C, Cambridge University Press, 2nd edn., 1992. 2556
Ridley, B. A., Grahek, F. E., and Walega, J. G.: A small, high-sensitivity, medium-response ozone detector suitable for measurements from light aircraft, J. Atmos. Ocean. Tech., 9, 142–148, 1992. 2543
Rohrer, F. and Brüning, D.: Surface NO and NO_2 mixing ratios measured between 30° N and 30° S in the Atlantic region, J. Atmos. Chem., 15, 253–267, 1992. 2543, 2544
Rohrer, F., Bohn, B., Brauers, T., Brüning, D., Johnen, F.-J., Wahner, A., and Kleffmann, J.: Characterisation of the photolytic HONO-source in the atmosphere simulation chamber SAPHIR, Atmos. Chem. Phys., 5, 2189–2201, 2005, http://www.atmos-chem-phys.net/5/2189/2005/. 2552
Rollins, A. W., Kiendler-Scharr, A., Fry, J. L., Brauers, T., Brown, S. S., Dorn, H.-P., Dubé, W. P., Fuchs, H., Mensah, A., Mentel, T. F., Rohrer, F., Tillmann, R., Wegener, R., Wooldridge, P. J., and Cohen, R. C.: Isoprene oxidation by nitrate radical: alkyl nitrate and secondary organic aerosol yields, Atmos. Chem. Phys., 9, 6685–6703, 2009,

http://www.atmos-chem-phys.net/9/6685/2009/. 2553
Ryerson, T. B., Williams, E. J., and Fehsenfeld, F. C.: An efficient photolysis system for fast-response NO_2 measurements, J. Geophys. Res., 105, 26447–26461, 2000. 2542, 2563
Schlosser, E., Bohn, B., Brauers, T., Dorn, H.-P., Fuchs, H., Häseler, R., Hofzumahaus, A., Holland, F., Rohrer, F., Rupp, L. O., Siese, M., Tillmann, R., and Wahner, A.: Intercomparison of two hydroxyl radical measurement techniques at the atmosphere simulation chamber SAPHIR, J. Atmos. Chem., 56, 187–205, doi:10.1007/s10874-006-9049-3, 2007. 2552
Shillings, A. J. L.: Atmospheric applications of broadband cavity ringdown spectroscopy, Phd thesis, University of Cambridge, 2009. 2550
Sonnenfroh, D. M. and Allen, M. G.: Ultrasensitive, visible tunable diode laser detection of NO_2, Appl. Optics, 35, 4053–4058, 1996. 2542
Thornton, J. A., Wooldridge, P. J., and Cohen, R. C.: Atmospheric NO_2: In situ laser-induced fluorescence detection at parts per trillion mixing ratios, Anal. Chem., 72, 528–539, doi:10.1021/ac9908905, 2000. 2542, 2544, 2545, 2546, 2563, 2564
Thornton, J. A., Wooldridge, P. J., Cohen, R. C., Williams, E. J., Hereid, D., Fehsenfeld, F. C., Stutz, J., and Alicke, B.: Comparisons of in situ and long path measurements of NO_2 in urban plumes, J. Geophys. Res., 108, 4496, doi:10.1029/2003JD003559, 2003. 2557
Vandaele, A. C., Hermans, C., Simons, P. C., Roozendael, M. v., Guilmot, J. M., Carleer, M., and Colin, R.: Fourier transform measurement of NO_2 absorption cross-sections in the visible range at room temperature, J. Atmos. Chem., 25, 189–305, 1996. 2549
Vandaele, A. C., Hermans, C., Fally, S., Carleer, M., Colin, R., Mérienne, M.-F., Jenouvrier, A., and Coquart, B.: High resolution fourier transform measurement of the NO_2 visible and near-infrared absorption cross section: Temperature and pressure effects, J. Geophys. Res., 107, 4348, doi:10.1029/2001JD000971, 2002. 2562
Varma, R. M., Venables, D. S., Ruth, A. A., Heitmann, U., Schlosser, E., and Dixneuf, S.: Long optical cavities for open-path monitoring of atmospheric trace gases and aerosol extinction, Appl. Optics B, 48, 159–171, 2009. 2551
Venables, D. S., Gherman, T., Orphal, J., Wenger, J., and Ruth, A. A.: High sensitivity in situ monitoring of NO_3 in an atmospheric simulation chamber using incoherent broad-band cavity-enhanced absorption spectroscopy, Environ. Sci. Technol., 40, 6758–6763, doi:10.1021/es061076j, 2006. 2542
Voigt, S., Orphal, J., and Burrows, J. P.: The temperature and pressure dependence of the absorption cross section of NO_2 in the 250–800 nm region measured by Fourier-transform

spectroscopy, J. Photochem. Photobiol., 149, 1–7, 2002. 2547, 2548, 2562

Wada, R. and Orr-Ewing, A. J.: Continuous wave cavity ring-down spectroscopy measurement of NO_2 mixing ratios in ambient air, Analyst, 130, 1595–1600, doi:10.1039/b511115c, 2005. 2542

Wegener, R., Brauers, T., Koppmann, R., Bares, S. R., Rohrer, F., Tillmann, R., Wahner, A., Hansel, A., and Wisthaler, A.: Simulation chamber investigation of the reactions of ozone with short-chained alkenes, J. Geophys. Res., 112, D13301, doi:10.1029/2006JD007531, 2007. 2552

Yokelson, R. J., Burkholder, J. B., Fox, R. W., Talukdar, R. K., and Ravishankara, A. R.: Temperature dependence of NO_3 absorption spectrum, J. Phys. Chem., 98, 13144–13150, 1994. 2547, 2548

Table 1. Chemical conditions during experiments conducted during the NO3Comp campaign. The mixing ratios given are maximum values during the experiments.

Date	NO_2/ppbv	O_3/ppbv	NO_3/pptv	N_2O_5/pptv	HNO_3/ppbv	H_2O/%	experiment/test
9 June	4	120	130	350	[a]	[b]	
10 June	4	230	170	300	0.7	0.5	stepwise change of humidity
11 June	17	100	150	750	1.2	1.8	addition of ambient air
12 June	8	200	400	1600	[a]	[b]	short photolysis events
13 June	18	200	700	2200	4	[b]	short photolysis events
14 June	12	135	180	850	6	[b]	oxidation of butanal (max. 4 ppbv)
15 June	10	180	120	550	2	1.8	addition of inorganic aerosol ($(NH_4)_2SO_4$)
16 June	38	60	55	1300	1.3	[b]	oxidation of limonene (max. 10 ppbv) +CO (max. 500 ppmv)
18 June	33	60	150	1400	4.5	1.2	oxidation of isoprene (max. 10 ppbv) +aerosol ($(NH_4)_2SO_4$)+CO (max. 500 ppmv)
20 June	75	100	400	5300	8	[b]	oxidation of β-pinene (max. 20 ppbv)
21 June	70	165	110	6000	3	1.2	oxidation of β-pinene (max. 20 ppbv)

[a] no valid measurements
[b] no addition of water vapor

AMTD
2, 2539–2586, 2009

Table 2. Results the linear regression analysis between NO_2 data of the PC-CLD instrument and LIF and CRDS (a: slope, b: intercept, R^2: correlation coefficient, χ^2: sum of weighted residuum, N: number of data points). Data are averaged to 1 min time intervals and the standard deviation is taken as error, unless the error propagation of the high resolution data was larger than the standard deviation. The small errors of the regression parameters indicate that deviations from a linear relationship between data sets cannot be explained by the error of measurements as reported for the instruments.

	LIF					CRDS				
date	a	b/ppbv	R^2	χ^2	N	a	b/ppbv	R^2	χ^2	N
9 June	1.073±0.007	0.05±0.02	0.99	154	110	1.029±0.009	−0.08±0.02	0.96	684	110
10 June	0.997±0.007	−0.03±0.01	0.99	136	92	0.997±0.004	−0.08±0.01	0.98	1970	124
11 June	0.943±0.004	0.33±0.04	>0.99	319	113	0.978±0.002	0.10±0.02	>0.99	303	121
12 June	0.989±0.006	0.13±0.02	0.99	386	148	0.955±0.003	−0.04±0.01	>0.99	800	160
13 June	1.018±0.004	0.04±0.03	0.99	327	81	0.998±0.002	−0.09±0.02	0.99	297	70
14 June	0.939±0.004	0.01±0.02	>0.99	157	124	1.018±0.002	−0.11±0.01	>0.99	428	153
15 June	0.964±0.006	0.03±0.02	>0.99	43	114	1.013±0.003	−0.21±0.01	>0.99	567	138
16 June	0.981±0.003	0.41±0.05	0.99	805	323	0.993±0.001	−0.70±0.04	>0.99	259	256
18 June	1.076±0.002	−0.28±0.03	0.99	1430	243	1.001±0.003	−0.46±0.04	>0.99	1360	283
20 June	0.979±0.002	0.48±0.08	>0.99	207	140	1.008±0.001	−0.18±0.08	>0.99	496	183
21 June	1.014±0.002	−0.06±0.06	>0.99	180	142	0.955±0.001	−0.20±0.08	>0.99	595	171
comb.	1.010±0.001	0.00±0.02	>0.99	7400	1630	0.982±0.001	−0.10±0.02	>0.99	13400	1769

Table 3. Same as Table 2 for NO_2 data of the BBCRDS and IBBCEAS instruments. Only experiments during which data were above the limit of detection are analyzed for BBCRDS measurements. Data from 10 June were excluded for the IBBCEAS instrument because instrumental parameters were optimized during this experiment.

	BBCRDS					IBBCEAS				
date	*a*	*b*/ppbv	R^2	χ^2	N	*a*	*b*/ppbv	R^2	χ^2	N
9 June						1.21±0.08	−0.98±0.18	0.90	24	160
11 June						0.85±0.02	1.13±0.15	0.98	52	149
12 June						0.989±0.008	0.04±0.03	0.96	676	185
13 June						1.45±0.01	0.98±0.09	0.99	114	160
14 June						1.117±0.008	−0.13±0.05	0.97	369	186
15 June						0.61±0.02	0.90±0.05	0.86	552	169
16 June						1.027±0.003	0.16±0.03	0.99	1330	447
18 June	0.59±0.04	7.5±0.6	0.28	381	87	1.048±0.007	−1.20±0.09	0.99	204	301
20 June	0.86±0.01	7.4±0.5	0.77	499	116	1.329±0.003	−0.28±0.10	>0.99	496	185
21 June	0.96±0.01	1.56±0.4	0.86	130	59	1.211±0.002	−0.66±0.08	0.99	2100	171
comb.	0.926±0.007	2.9±0.2	0.81	1250	262	1.191±0.001	−0.47±0.02	0.98	33600	2113

AMTD
2, 2539–2586, 2009

Table 4. Estimation of the detection limit for instruments from Allan deviation plot for a signal to noise ratio of two from zero air sampling for 10 s averaged data (except for PC-CLD). The precision $\langle\sigma_{fit}\rangle$ of measurements was calculated as standard deviation of the residuum of an exponential fit to the data for periods when either only NO_2, or NO_2 and O_3 was present is compared to the mean of the reported error of the data $\langle\sigma_{data}\rangle$ (see text for details). The accuracy of instruments is given as stated by the group operating the instrument.

	LOD/pptv	$\langle\sigma_{fit}\rangle/\langle\sigma_{data}\rangle$	time resolution/s	1σ accuracy / %
BBCRDS	[a]	[a]	61	11
CRDS	80 (10 s)	1.2	1	6
IBBCEAS	600 (10 s)	0.5	5	18
LIF	100 (10 s)	0.5	10	5
PC-CLD	10 (180 s)	[a]	180	7

[a] insufficient number of data points

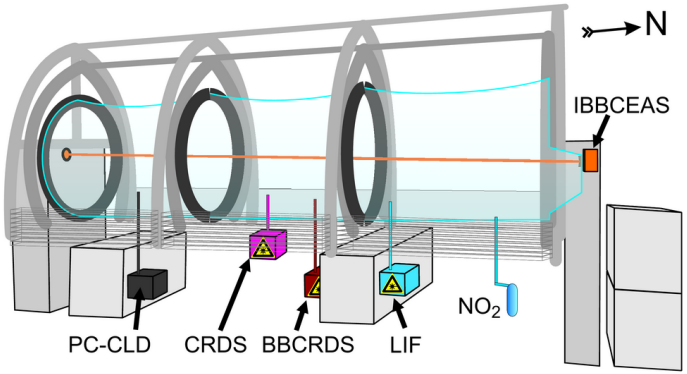

Fig. 1. Setup of instruments detecting NO_2 at SAPHIR. Color of instruments refer to the colors used in Figs. 2–4. The IBBEAS transmitter and receiver were located at opposite ends of the chamber.

AMTD
2, 2539–2586, 2009

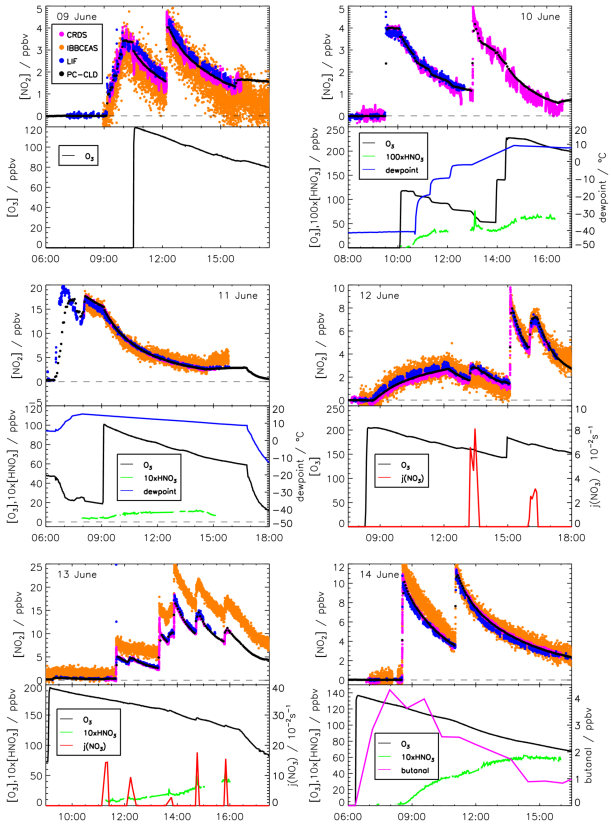

Fig. 2. Time series of NO_2 mixing ratios from all instruments at their original time resolution (BBCRDS: 61 s, CRDS: 1 s, IBBCEAS 5 s, LIF: 10 s, PC-CLD: 180 s) for experiments between 9 June and 14 June. All reported data are shown. Ozone was measured by a chemiluminescence detector, water vapor by dew point hygrometer, nitric acid by LOPAP, photolysis frequency by spectroradiometer and butanal by a GC FID system.

AMTD
2, 2539–2586, 2009

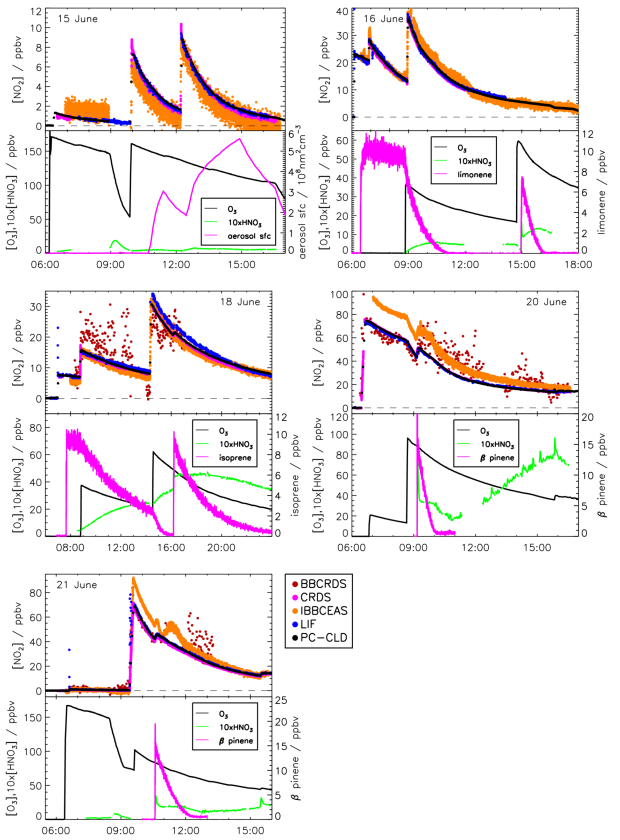

Fig. 3. Same as Fig. 2. In addition aerosol surface area measured by SMPS and mixing ratios and limonene, isoprene and β-pinene measured by PTRMS is shown.

AMTD
2, 2539–2586, 2009

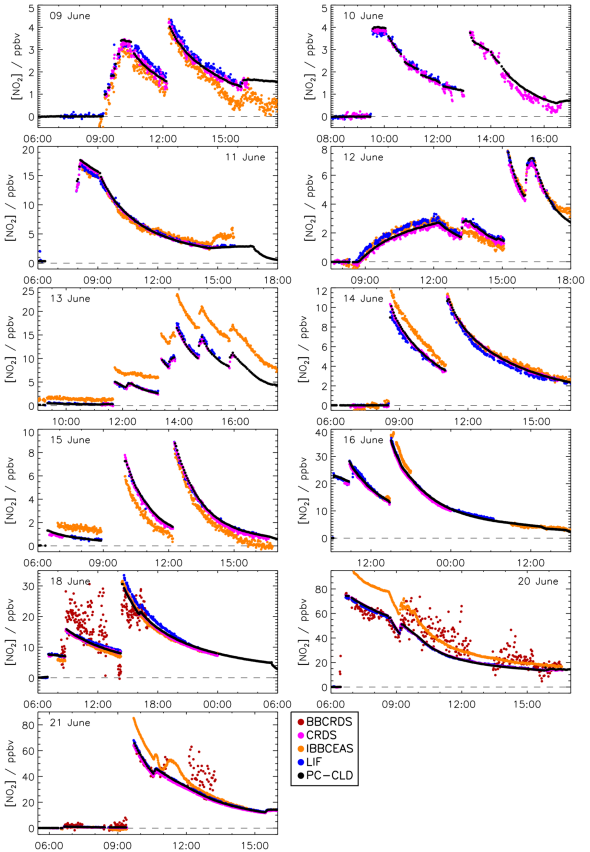

Fig. 4. Time series of NO_2 mixing ratios from all instruments. Data were averaged to a 1 min time resolution, if the original data set provided a higher temporal resolution. Only data which are used for the analysis are shown, e.g. data during the addition of trace gases were rejected in the analysis because of potential inhomogeneities of the trace gas in the chamber.

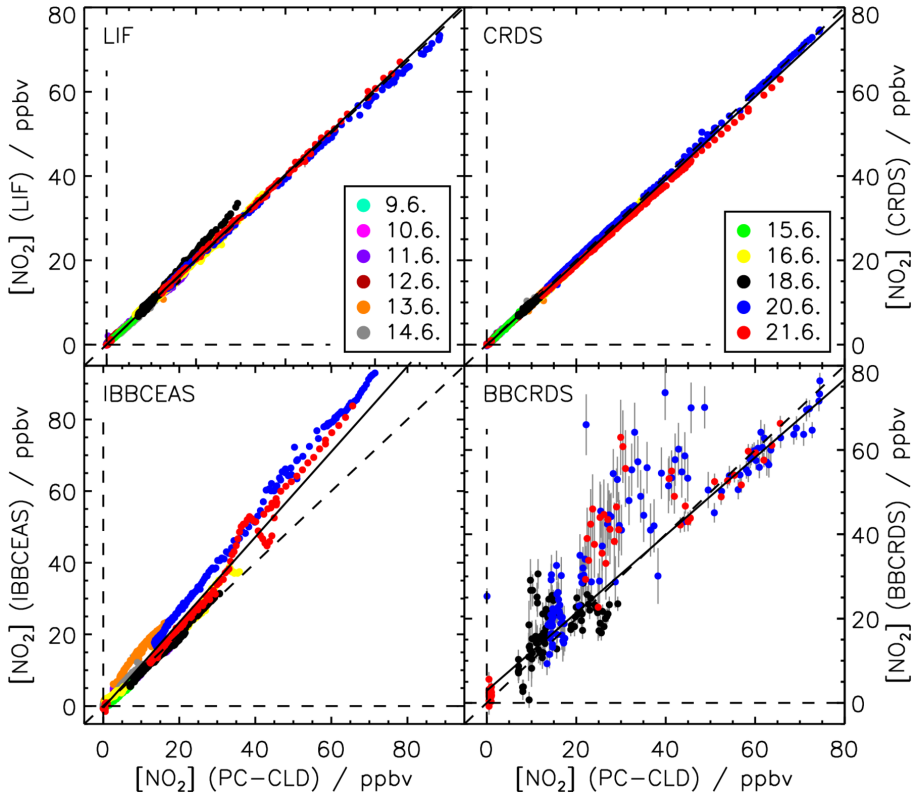

Fig. 5. Correlation plots between NO_2 mixing ratios from BBCRDS, CRDS, IBBCEAS and LIF with NO_2 mixing ratios from the PC-CLD as reference. X- and y-error bars are smaller than the symbol size for some of the data points. The solid black line indicates the fit line from the regression analysis for the whole data set from all experiments and the dashed line is the 1:1 line.

AMTD
2, 2539–2586, 2009

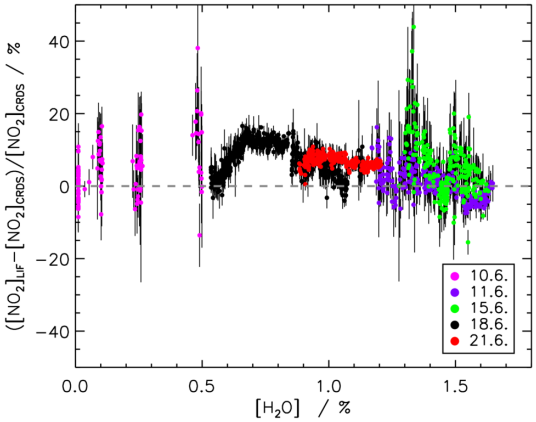

Fig. 6. Relative difference between NO_2 mixing ratio measured by LIF and CRDS (1 min time resolution) depending on the water vapor (measured by a dewpoint hygrometer) present in the chamber. Only experiments during which water vapor was added are included.

AMTD
2, 2539–2586, 2009

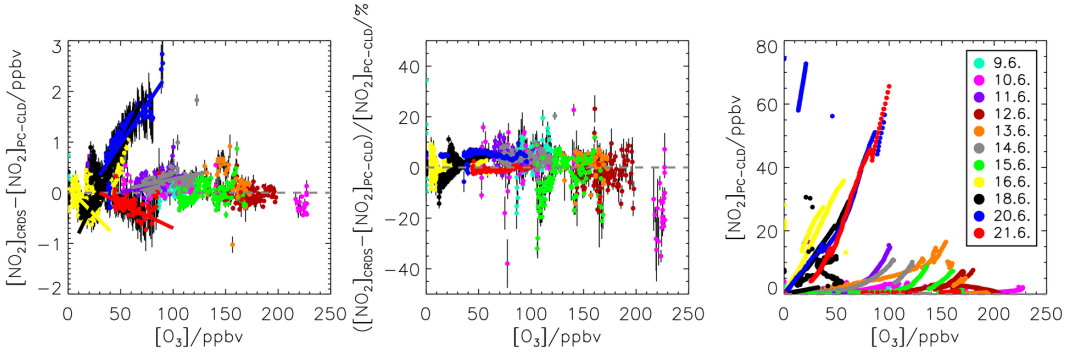

Fig. 7. Absolute (left panel) and relative (center panel) difference between NO_2 mixing ratio measured by CRDS and PC-CLD (at the time resolution of the PC-CLD instrument) depending on the ozone mixing ratio present in the chamber. NO_2 and O_3 (right panel) are highly correlated, so that trends in the difference between CRDS and PC-CLD measurements cannot be unambiguously attributed to errors in the ozone correction of CRDS.

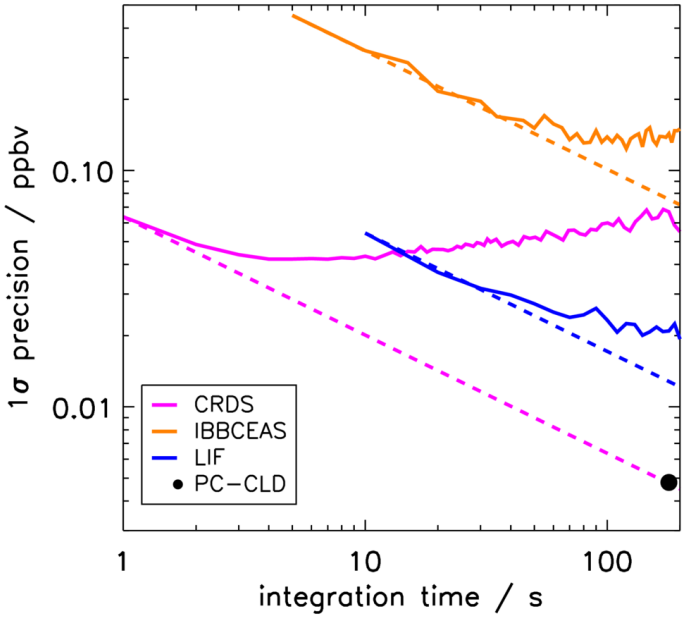

Fig. 8. Dependence of 1σ precision (solid lines) on integration time (Allan deviation plot) from periods of zero air sampling. Dashed lines is the precision expected for purely random noise. The number of data points was insufficient to calculate the Allan deviation for the BBCRDS instrument. For the PC-CLD the number of zero air measurements was too small to calculate the Allan deviation for longer integration times than for its native time resolution.

AMTD
2, 2539–2586, 2009